Methane-Assisted Catalytic Desulfurization in an Environmentally Benign Way

Hua Song (sonh@ucalgary.ca)
University of Calgary https://orcid.org/0000-0002-2791-1723
Hao Xu
University of Calgary
Peng He
Synfuels China Technology Co. Ltd.
Zhaofei Li
University of Calgary
Shijun Meng
Yimeng Li
University of Calgary
Lo-Yueh Chang
National Synchrotron Radiation Research Center
Lijia Liu
Western University
Xiaodong Wen
Institute of Coal Chemistry & Synfuels China Company Limited https://orcid.org/0000-0001-5626-8581
Brittney Klein
University of Alberta
Vladimir Michaelis
Massachusetts Institute of Technology https://orcid.org/0000-0002-6708-7660
Jizhen Qi
Suzhou Institute of Nano-Tech and Nano-Bionics (SINANO), Chinese Academy of Sciences
Dongchang Wu
Thermo Fisher
Xi Liu
SynCat@Beijing, Synfuels China Technology Co.

Physical Sciences - Article

Keywords: petroleum, catalysis, methane-assisted catalytic desulfurization

Posted Date: June 15th, 2021

DOI: https://doi.org/10.21203/rs.3.rs-280255/v1

Abstract

Petroleum is one of the most important natural resources for human beings, while the contained sulfur heteroatoms lead to a series of problems1. Therefore, a desulfurization process to reduce sulfur content is mandatory for clean petroleum utilization. Hydrodesulfurization is currently mature in industry, while this process is costly, energy intensive and environmentally unfriendly due to CO2 emission and H2S production2,3. Alternative cost-effective desulfurization process with environmentally benign sulfur-containing products remains unreported. Here we demonstrate that the desulfurization of a heavy oil model compound dibenzothiophene can be successfully achieved under methane environment over creatively designed dual catalyst system, generating a new sulfur-containing product CS2. Control experiments indicate that the presence of methane as well as catalyst components for direct desulfurization and methane activation are all required. The reaction process is better understood by extensive evidences from isotope labeling experiments, catalyst and product characterizations, density functional theory calculations and verification experiments, based on which a reasonable catalytic mechanism is proposed. It is found that methane-assisted desulfurization requires more stringent conditions, where sulfur vacancy abundance, methane activation capability and surface sulfur transfer are all indispensable. This study pioneers a transformational desulfurization route, which is more economically and environmentally attractive for petroleum processing industry.

Main Text

Sulfur could be the most abundant heteroatoms in crude oil with the content ranging from 0.5 wt% to 6 wt%, leading to a series of problems such as sulfur oxide (SO_x) emission and acid rain[1,4,5]. With the increasing awareness of environmental protection, a desulfurization process to remove sulfur heteroatoms for downstream utilization becomes a must for clean energy utilization and corresponding legislations came into effect consecutively[6]. For example, the maximum sulfur content tolerance of 15 ppm was applied to on-road vehicles, non-road vehicles and locomotives in North America in 2006, 2010 and 2012, respectively, and more strict limitation of 10 ppm in gasoline came into effect in 2017[7]. Starting from 2020, a new regulation implemented by International Maritime Organization further lowered the acceptable sulfur content in marine oil used by ships outside designated emission control areas from 3.5 wt% to 0.5 wt%[8]. Conventional desulfurization process generally uses H_2 for effective sulfur removal and is thus called hydrodesulfurization (HDS), during which H_2 acts as the reductant and H_2S is formed as the product[3,9]. H_2 is generally produced from methane reforming process, which is energy intensive due to the stringent reaction conditions (950-1100 ^oC, 100 atm). The byproduct CO_2 also leads to greenhouse gas emission[9,10]. Besides, H_2S is notoriously famous for its high toxicity and environmental unfriendliness[11,12]. Therefore, the HDS route is environmentally and economically unfavorable. Methane is widely present as the main constituent in natural resources such as natural gas[13]. In recent years, the production of natural gas is increasing and the price is decreasing correspondingly (from 8.85 USD/Million British Thermal Units at Henry Hub in 2008 to 2.33 in 2020)[14,15]. If methane is used directly

for desulfurization process, the undervalued methane resources can be better utilized and the aforementioned reforming process can be avoided[16,17]. Besides, it would be highly preferred if other environmentally benign sulfur products rather than H_2S can be generated. It is clear that the methane-assisted desulfurization process (MDS) can be a transformational route for clean oil production. Dibenzothiophene (DBT) is one of the most commonly found sulfur-containing components in petroleum, especially in heavy oil[18,19]. It is widely accepted as a model compound for the study of heavy oil and is notably persistent to desulfurization due to the stable fused-ring structure[20]. Therefore, if DBT desulfurization is realized under methane environment, it is highly possible that other sulfur-containing species in crude oil can also be effectively converted. The chemistry involved could further provide valuable insights regarding possibilities and pathways to deal with unfavorable substances in a cost effective and environmentally benign way.

It is fully demonstrated in this proof-of-concept work that methane-assisted desulfurization is technically achievable over rationally designed dual catalyst system consisting of MDS1 catalyst ($NiMoS/TiO_2$) for direct desulfurization and MAC1 catalyst (AgGaCe/ZSM-5) for methane activation (Fig. 1(a)). An environmentally benign sulfur-containing product carbon disulfide (CS_2) is formed, which has never been publicly reported to the best of our knowledge. Control experiments prove that the presence of methane, MDS1 and MAC1 are all requisite for this ground-breaking desulfurization route. ^{13}C isotope labeling experiments suggest the participation of activated methane in the reaction, while ^{34}S isotope experiments indicate that the sulfur atom in DBT gets adsorbed and interchanged with sulfur vacancies in MDS1, triggering the subsequent reactions. Characterization of catalysts and products, extra confirmation experiments and DFT calculations are further performed and a validated reaction mechanism is proposed. It can be seen that different from hydrodesulfurization process, the methane-assisted desulfurization requires much more stringent conditions since the abundance of sulfur vacancies, the capability of methane activation and the surface sulfur transfer process are all indispensable. Therefore, unique catalyst design strategies are essential to this transformational MDS process, which has great potential to be much more economically feasible and environmentally friendly for petroleum industry.

DBT desulfurization under methane environment was carried out over a dual catalyst system (entry 1). The design of the catalyst system is explained in Section 2.1 and 2.2 of the Supplementary Information. The overall analysis results with estimated error ranges are shown in Table S3. Acceptable mass, carbon and sulfur balances are verified in Table S4, and the detailed distribution of converted reactants and formed products are shown in Fig. 1(b). In entry 1, 1.4% methane conversion and 14.0% DBT conversion are realized, which cannot be fully attributed to experimental error, evidently showing the occurrence of reaction. In gas phase, ethane is observed as the main product and trace amount of H_2 is detected. However, H_2S is not detected in gas phase, which is particularly different from the traditional HDS process. In soluble phase, CS_2 is clearly observed as a product, which is distinctive in the MDS process. Comparing with H_2S, CS_2 has much lower toxicity, which is widely used as an environmentally benign solvent and intermediate for organic synthesis[21-23]. Therefore, the production of CS_2, although the

amount is temporarily limited, deserves extra attentions. Besides, considerable quantities of other valuable products such as benzene, toluene and xylenes (BTX) are also witnessed. These products might originate from the decomposition of biphenyl, which is also observed as a product and widely reported in the direct desulfurization (DDS) pathway of the HDS process, indicating the presence of DDS reactions[24]. Other detectable products include benzene and biphenyl derivatives with various side chain substituents, which might be generated through alkylation reactions. However, typical products generated from the hydrogenation (HYD) pathway of the HDS process such as cyclohexylbenzene are not observed, confirming the absence of HYD reactions in the MDS process[24]. Besides, the presence of high boiling point soluble products confirmed by simulated distillation (Fig. S3) and coke confirmed by thermalgravimetric analysis (Fig. S4) suggest the occurrence of polymerization and coking reactions.

Control experiments (entry 2~4) were further performed and the overall analysis results are shown in Table S5. The distribution of converted reactants and formed products are further compared with entry 1 in Fig. 1(b). Comparing entry 1 and entry 2 (no CH_4), it is evident that much more types and amounts of soluble products are generated with the presence of methane, which cannot be realized under nitrogen environment, indicating the importance of methane to participate in the reaction and form valuable products. It is worth noting that the facilitation of DBT desulfurization after methane introduction leads to the co-utilization of methane and sulfur-containing compounds, converting intractable and low value-added reactants to valuable products, which is highly meaningful in both economic and environmental aspects. Comparing entry 1 and entry 3 (no MAC1), it can be seen that methane conversion decreases dramatically without MAC1, suggesting the essential role of MAC1 for methane activation. Considering the inert nature of methane due to its stable structure and high C-H bond energy of 435 kJ mol^{-1} (the highest among hydrocarbons), this conclusion is undoubtably reasonable: different from the intrinsic high activity of H_2 in the HDS process, a rationally designed catalyst for methane activation is critical for triggering the MDS process[25,26]. The conclusion also explains the lack of reports on the MDS process so far, since the feasibility is extremely low if a conventional HDS catalyst is solely employed, which is not capable of methane activation. Comparing entry 1 and entry 4, although methane conversion can be even higher over MAC1 in the absence of MDS1, the activated methane molecules are almost fully converted to ethane since the mass of converted methane is similar to that of produced ethane. The predominant formation of ethane can be explained by the self-combination of methyl radicals after methane activation, which is commonly reported in our previous studies[27,28]. Looking back to entry 1, it can be deduced that the presence of MDS1 opens up a new desulfurization pathway, which competes with the formation of ethane. Therefore, MDS1 is also indispensable for effective conversion of DBT to environmentally benign CS_2 and other valuable sulfur-free products.

To further rationalize active components in MDS1 and MAC1, more control experiments were designed and the results are shown in Table S6 and Fig. 1(c). Entry 1-O is a control experiment using MDS1-O catalyst, which is the oxide form of MDS1. The product distribution in entry 1-O is similar to that in entry 4 while totally different from that in entry 1, suggesting that the sulfide-form catalyst MDS1 cannot be replaced by an oxide-form counterpart. This might be due to the fact that appropriate active sites for

desulfurization, which are widely reported as sulfur vacancies, only exist on the surface of sulfide-form catalysts[29,30]. Besides, MAC2 (no Ag), MAC3 (no Ce) and MAC4 (no Ga) were evaluated to investigate the function of metals in MAC1. According to Fig. 1(c), MAC2 and MAC3 leads to similar conversion of reactants and product distribution. The yields of desulfurized products such as biphenyl and BTX are close to those in entry 1, indicating the desulfurization reaction still goes on smoothly. However, much lower CS_2 yield is observed in these two entries, suggesting the active roles of Ag and Ce for the formation of CS_2. Moreover, methane conversion and the yields of desulfurized products are extremely limited in entry 1-MAC4, indicating methane is not fully activated without Ga. The conclusion that Ga is essential for methane activation is also repeatedly reported in previous work[31,32].

To further reveal the evolution of methane in the reaction process, an isotope labeling reaction entry1-13C was carried out using ^{13}C concentrated methane. The soluble product was analyzed by gas chromatography-mass spectrometry (GC-MS) and ^{13}C nuclear magnetic resonance (NMR), and the results are illustrated in Fig. 2, Fig. S5 and Table S7. According to the mass spectra in Fig. 2(a~c), the distributions of m/z for monocyclic aromatic products clearly shift to the higher end in entry 1-13C compared to those in entry 1, indicating methane incorporation in these products. The signal increase rate follows the order xylene (310 %) > toluene (234%) > benzene (181%), suggesting the ^{13}C atoms from $^{13}CH_4$ are incorporated preferably on the side chain as methyl groups rather than in the aromatic ring. This conclusion is further supported by liquid ^{13}C NMR analysis in Fig. S7. However, the signal increase rate of CS_2 is only 11%, implying that the carbon atoms in CS_2 should not be fully from methane (Fig. 2(d)). Moreover, no signal increase is observed for biphenyl, indicating that the carbon atoms in biphenyl might fully come from DBT (Fig.2 (e)). The unique ^{13}C distribution provides extra evidence for the reaction mechanisms.

To further substantiate the important role of sulfide catalyst in desulfurization process, entry 1-S and entry 1-34S were carried out using the catalyst derived from natural elemental S and ^{34}S, respectively. According to Fig. 2(f), the ratios of m/z intensities 78/76 (0.049) and 80/78 (0.042) for CS_2 in entry 1-S conform well with natural sulfur isotope abundance (^{34}S:^{32}S=0.043). However, it is clearly seen that the intensities of m/z at 78 and 80 (correspond to $C^{32}S^{34}S$ and $C^{34}S_2$) increase in entry 1-34S dramatically, indicating the incorporation of S atoms from catalyst in the final CS_2 product, which can be attributed to the sulfur exchange between ^{32}S captured from DBT and ^{34}S initially present in the isotope-labeled catalyst. This sulfur exchange is also reported to be critical for the HDS process in previous studies[33,34].

The fresh and used MDS1 and MAC1 catalysts were systematically characterized and the results are summarized in Fig. 3 and Fig. S6~S14. The sulfur capturing capability of MDS1 is further confirmed by X-ray adsorption fine structure (XAFS) study as shown in Fig. 3(a) and Fig. S6. According to Fig. 3(a), the patterns of Mo K-edge in sample MDS1-O are similar to those in MoO_3 standard, confirming its oxide nature. However, the features in MDS1 and MDS1-Used are different from those in MoO_3 and MoS_2,

which seem to be a combination of both. The fitting results in Table S8 substantiate that the coordination number of Mo-S in MDS1 is much lower than the theoretical value of 6, suggesting the presence of sulfur vacancies. Meanwhile, the coordination number of Mo-S increases significantly in MDS1-Used, proving that sulfur atoms from DBT have been captured by the sulfur vacancies of MDS1. Similar conclusions can be drawn from Ni K-edge and S K-edge spectra (Fig. S6 and Table S9). Microstructural analysis of molybdenum sulfide in fresh and used MDS1 catalysts is further discussed in Fig. S9~S12.

X-ray photoelectron spectroscopy (XPS) results in Fig. 3(b) clearly suggest that Ag in MAC1-Used is sulfurized. Besides, local energy-dispersive X-ray spectroscopy (EDX) mapping results validate the co-existences of Ag-S and Ce-S in MAC1-Used (Fig. 3(c~e) and Fig. S13(b)). Therefore, although desulfurization occurs primarily over MDS1, a sulfur transfer process from MDS1 to MAC1 also takes place with the assistance of Ag and Ce during the reaction.

The formation of CS_2 is further supported by advanced scanning/transmission electron microscopy (STEM). In order to visualize the beam-sensitive porous structure of ZSM-5 and identify chemical compositions of absorbents in MAC1, integrated differential phase contrast (iDPC) STEM technique was employed to image fresh and used MAC1 catalysts. The framework of ZSM-5 is clearly seen from the [010] projection with atomic resolution in Fig. 3(g~h), which is in good agreement with theoretical model and previous TEM work[35]. In contrast to empty channels of the fresh catalyst in Fig. 3(g), channels of the used one are almost fully occupied by light absorbent molecules. The carbon and sulfur signals can be clearly identified in both integrated STEM-EELS (electron energy loss spectroscopy, Fig. 3(f)) and EDX spectra (Fig. S14(c)), which were collected from the ZSM-5 areas without sulfurized Ag or Ce compounds (Fig. S14(a~b)). These observations rationalize that the absorbent molecules should be carbon-sulfur compounds, suggesting that CS_2 might be formed and the process might occur preferably over MAC1.

The reaction mechanism was further explored by carefully designed verification experiments (Table S10~S16). Vial-separated experiments (Table S10) where MDS1 and MAC1 are physically separated further differentiate the function of MDS1 and MAC1: the yields of BTX and biphenyl are higher over MDS1 than over MAC1, while the yields of other aromatics and coke are higher over MAC1 than over MDS1. These results suggest that DBT desulfurization and biphenyl decomposition mainly occur over MDS1, while alkylation take place preferably over MAC1. This conclusion is further corroborated by $^{13}C\{^1H\}$ solid-state cross-polarization magic angle spinning nuclear magnetic resonance (SS CP/MAS NMR) spectra (Fig. 3(i)) and other verification experiments (Table S11~S13). The preferred adsorptions of DBT over MDS1 and CH_4 over MAC1 are also supported by density functional theory (DFT) calculations (Fig. 4(a~b)). Besides, the absence of CS_2 in vial-separated experiments also suggests that sulfur transfer from MDS1 to MAC1 is a surface process, which does not occur in the gas phase.

Based on all experiments, characterization and calculation results, a catalytic reaction mechanism is proposed as shown in Fig. 1(a). First, DBT is adsorbed on the sulfur vacancies over MDS1 (supported by Fig. 3(a), 4(a), S6, Table S8 and S9) and methane is activated by Ga over MAC1 (supported by Fig. 3(i),

4(b) and Table S11). Then, the radicals generated upon methane activation interact with DBT over MDS1 through the DDS pathway (supported by Fig. 4(c) and Table S15) to form an important sulfur-free product biphenyl and S atoms (supported by Fig. S6 and Table S10). Later, biphenyl participates in a series of reactions including decomposition and alkylation, resulting in the formation of other aromatic products such as BTX (supported by Fig. 3(i) and Table S12). Meanwhile, a surface sulfur transfer process from MDS1 to MAC1 occurs with the assistance of Ag and Ce (supported by Fig. 3(b~e) and Table S10). Subsequently, methyl group generated over MAC1 further triggers hydrogen transfer reactions and produces free C atoms, and the latter react with transferred S atoms to form the final sulfur-containing product CS_2 (supported by Fig. 3(f~h), Table S14 and S16). Besides, it should be noted that a series of side reactions, such as ethane formation (supported by Table S11), coking (supported by Table S10~S14), methylation (supported by Table S10 and S13), methyl exchange and ring expansion-contraction of aromatics (supported by Fig. 2(a~c)) are also going on during the process, leading to more diverse product distribution as shown in Fig. 1(b). These side reactions are not shown in Fig. 1(a) for clarity. From this surface reaction network, it is clear that MDS1 and MAC1 are also indispensable for successful MDS process. It is worth noting that it is the creative catalyst design that enables the possibility of methane-assisted DBT desulfurization, which pioneers a new pathway for dealing with sulfur heteroatoms and generating new sulfur-containing product CS_2 with unique economic and environmental advantages.

Declarations

Acknowledgments

The authors gratefully acknowledge the financial supports from Kara Technologies Inc., Natural Sciences and Engineering Research Council of Canada (NSERC) through collaborative research and development program (CRDPJ/531607-18), Alberta Innovates (AI 2552) and NFRF. X. Liu acknowledges the financial supports from National Natural Science Foundation of China (Grant Nos. 21872163, 22072090, 21991153, 21991150). The authors also appreciate technical support from Mr. Hiroaki Matsumoto and Mr. Chaobin Zeng from Hitachi High-Technologies (Shanghai) Co. Ltd, for HR-STEM/Hr-SE characterizations.

Author contributions

H. Xu performed the reactions, analyzed the data and wrote the manuscript. H. Xu and Z. Li performed the isotope labeling experiments. H. Xu and Y. Li performed the sulfur content measurement of solid and liquid samples. P. He and X. Wen performed the liquid ^{13}C NMR and XPS experiments. L. Chang performed the XAFS characterizations. L. Liu analyzed the XAFS data. B. A. Kleine and V. K. Michaelis performed the SS CP/MAS NMR characterizations and analyzed the corresponding data. X. Liu and J. Qi conducted the STEM characterization and analyzed the corresponding data. D. Wu provided technical supports for iDPC characterizations. H. Xu and S. Meng performed the DFT calculations. H. Song

designed the experiments and administrated the project. X. Liu and H. Song supervised the research. All authors revised the manuscript.

Competing interests

The authors declare no competing interests.

References

1 Yang, R. T., Hernandez-Maldonado, A. J. & Yang, F. H. Desulfurization of Transportation Fuels with Zeolites Under Ambient Conditions. *Science* **301**, 79-81 (2003).

2 Bonneau, P. R., Jr, R. F. J. & Kaner, R. B. Rapid solid-state synthesis of materials from molybdenum disulphide to refractories. *Nature* **349**, 510-512 (1991).

3 Brunet, S., Mey, D., Pérot, G., Bouchy, C. & Diehl, F. On the hydrodesulfurization of FCC gasoline: a review. *Applied Catalysis A: General* **278**, 143-172, doi:10.1016/j.apcata.2004.10.012 (2005).

4 Amoatey, P., Omidvarborna, H., Baawain, M. S. & Al-Mamun, A. Emissions and exposure assessments of SOX, NOX, PM10/2.5 and trace metals from oil industries: A review study (2000–2018). *Process Safety and Environmental Protection* **123**, 215-228, doi:10.1016/j.psep.2019.01.014 (2019).

5 Zipper, C. E. & Gilroy, L. Sulfur Dioxide Emissions and Market Effects under the Clean Air Act Acid Rain Program. *J Air Waste Manag Assoc* **48**, 829-837, doi:10.1080/10473289.1998.10463731 (1998).

6 Kumar, S., Srivastava, V. C. & Nanoti, S. M. Extractive Desulfurization of Gas Oils: A Perspective Review for Use in Petroleum Refineries. *Separation & Purification Reviews* **46**, 319-347, doi:10.1080/15422119.2017.1288633 (2017).

7 Mallidis, I., Despoudi, S., Dekker, R., Iakovou, E. & Vlachos, D. The impact of sulphur limit fuel regulations on maritime supply chain network design. *Annals of Operations Research* **294**, 677-695, doi:10.1007/s10479-018-2999-4 (2018).

8 Alshammari, Y. M. & Benmerabet, M. Global scenarios for fuel oil utilisation under new sulphur and carbon regulations. (2017).

9 Tanimu, A. & Alhooshani, K. Advanced Hydrodesulfurization Catalysts: A Review of Design and Synthesis. *Energy & Fuels* **33**, 2810-2838, doi:10.1021/acs.energyfuels.9b00354 (2019).

10 Xu, R., Chou, L.-C. & Zhang, W.-H. The effect of CO2 emissions and economic performance on hydrogen-based renewable production in 35 European Countries. *International Journal of Hydrogen Energy* **44**, 29418-29425, doi:10.1016/j.ijhydene.2019.02.167 (2019).

11 Liu, D., Li, B., Wu, J. & Liu, Y. Sorbents for hydrogen sulfide capture from biogas at low temperature: a review. *Environmental Chemistry Letters* **18**, 113-128, doi:10.1007/s10311-019-00925-6 (2019).

12 Lincke, M. *et al.* Chemoadsorption for Separation of Hydrogen Sulfide from Biogas with Iron Hydroxide and Sulfur Recovery. *Chemical Engineering & Technology* **43**, 1564-1570, doi:10.1002/ceat.202000032 (2020).

13 Liang, Z., Li, T., Kim, M., Asthagiri, A. & Weaver, J. F. Low-temperature activation of methane on the IrO2(110) surface. *Science* **356**, 299-303 (2017).

14 BP Statistical Review of World Energy. (BP Energy Economics, 2019).

15 Davis, C. BP Bearish on Natural Gas Prices, LNG Exports to 2021. (2019).

16 Díaz-Urrutia, C. & Ott, T. Activation of methane: A selective industrial route to methanesulfonic acid. *Science* **363**, 1326-1329 (2019).

17 Roytman, V. A. & Singleton, D. A. Comment on “Activation of methane to CH3 industrial route to methanesulfonic acid”. *Science* **363**, 1326-1329, doi:10.1002/anie.200350976 (2019).

18 Jia, S. Y. *et al.* Adsorptive removal of dibenzothiophene from model fuels over one-pot synthesized PTA@MIL-101(Cr) hybrid material. *Journal of hazardous materials* **262**, 589-597, doi:10.1016/j.jhazmat.2013.08.056 (2013).

19 Zhang, C. *et al.* Synthesis, Characterization, and Evaluation of Activated Carbon Spheres for Removal of Dibenzothiophene from Model Diesel Fuel. *Industrial & Engineering Chemistry Research* **53**, 4271-4276, doi:10.1021/ie403773f (2014).

20 Rabarihoela-Rakotovao, V., Brunet, S., Perot, G. & Diehl, F. Effect of H2S partial pressure on the HDS of dibenzothiophene and 4,6-dimethyldibenzothiophene over sulfided NiMoP/Al2O3 and CoMoP/Al2O3 catalysts. *Applied Catalysis A: General* **306**, 34-44, doi:10.1016/j.apcata.2006.03.029 (2006).

21 Samoc, A. Dispersion of refractive properties of solvents: Chloroform, toluene, benzene, and carbon disulfide in ultraviolet, visible, and near-infrared. *Journal of Applied Physics* **94**, 6167-6174, doi:10.1063/1.1615294 (2003).

22 Ishizuka, T., Takanohashi, T., Ito, O. & Iino, M. Effects of additives and oxygen on extraction mixed solvent for Argonne premium coal samples yield. *Fuel* **72**, 579-580 (1992).

23 Fukuda, H. & Oda, M. Copolymerization of Ketene Cyclic N,O-Acetals with Carbon Disulfide: Evidence for Formation of Zwitterionic Intermediates by Means of 1H NMR Spectroscopy. *Macromolecules* **29**, 3043-3045 (1996).

24 Signhal, G. H., Espino, R. L., Sobel, J. E. & Huff, G. A. Hydrodesulfurization of Sulfur Heterocyclic Compounds. *Journal of Catalysis* **67**, 457-458 (1981).

25 Choudhary, V. R., Kinage, A. K. & Choudhary, T. V. Low-Temperature Nonoxidative Activation of Methane over H-Galloaluminosilicate (MFI) Zeolite. *Science* **275**, 1286-1288 (1997).

26 Maugh, T. H., 2nd. Methane C-h bonds activated. *Science* **222**, 315, doi:10.1126/science.222.4621.315 (1983).

27 He, P., Jarvis, J., Liu, L. & Song, H. The promoting effect of Pt on the co-aromatization of pentane with methane and propane over Zn-Pt/HZSM-5. *Fuel* **239**, 946-954, doi:10.1016/j.fuel.2018.11.079 (2019).

28 He, P. *et al.* Co-aromatization of methane with propane over Zn/HZSM-5: The methane reaction pathway and the effect of Zn distribution. *Applied Catalysis B: Environmental* **250**, 99-111, doi:10.1016/j.apcatb.2019.03.011 (2019).

29 Sharifvaghefi, S., Yang, B. & Zheng, Y. New insights on the role of H2S and sulfur vacancies on dibenzothiophene hydrodesulfurization over MoS2 edges. *Applied Catalysis A: General* **566**, 164-173, doi:10.1016/j.apcata.2018.05.033 (2018).

30 Guo, K., Ding, Y., Luo, J. & Yu, Z. Nickel Cobalt Thiospinel Nanoparticles as Hydrodesulfurization Catalysts: Importance of Cation Position, Structural Stability, and Sulfur Vacancy. *ACS Appl Mater Interfaces* **10**, 19673-19681, doi:10.1021/acsami.8b03588 (2018).

31 He, P., Gatip, R., Yung, M., Zeng, H. & Song, H. Co-aromatization of olefin and methane over Ag-Ga/ZSM-5 catalyst at low temperature. *Applied Catalysis B: Environmental* **211**, 275-288, doi:10.1016/j.apcatb.2017.04.052 (2017).

32 Li, Q. *et al.* Catalytic co-aromatization of methane and heptane as an alkane model compound over Zn-Ga/ZSM-5: A mechanistic study. *Applied Catalysis B: Environmental* **236**, 13-24, doi:10.1016/j.apcatb.2018.05.006 (2018).

33 Paál, Z., Koltai, T. & late) Károly, M. Sulfur uptake and exchange, HDS activity and structure of sulfided, Al2O3 supported MoOx, PdMoOx and PtMoOx catalysts. *Physical Chemistry Chemical Physics* **3**, 1535-1543, doi:10.1039/b009047f (2001).

34 Sushkevich, V. L., Popov, A. G. & Ivanova, II. Sulfur-33 Isotope Tracing of the Hydrodesulfurization Process: Insights into the Reaction Mechanism, Catalyst Characterization and Improvement. *Angewandte Chemie* **56**, 10872-10876, doi:10.1002/anie.201704027 (2017).

35 Shen, B. *et al.* Atomic Spatial and Temporal Imaging of Local Structures and Light Elements inside Zeolite Frameworks. *Adv Mater* **32**, e1906103, doi:10.1002/adma.201906103 (2020).

Figures

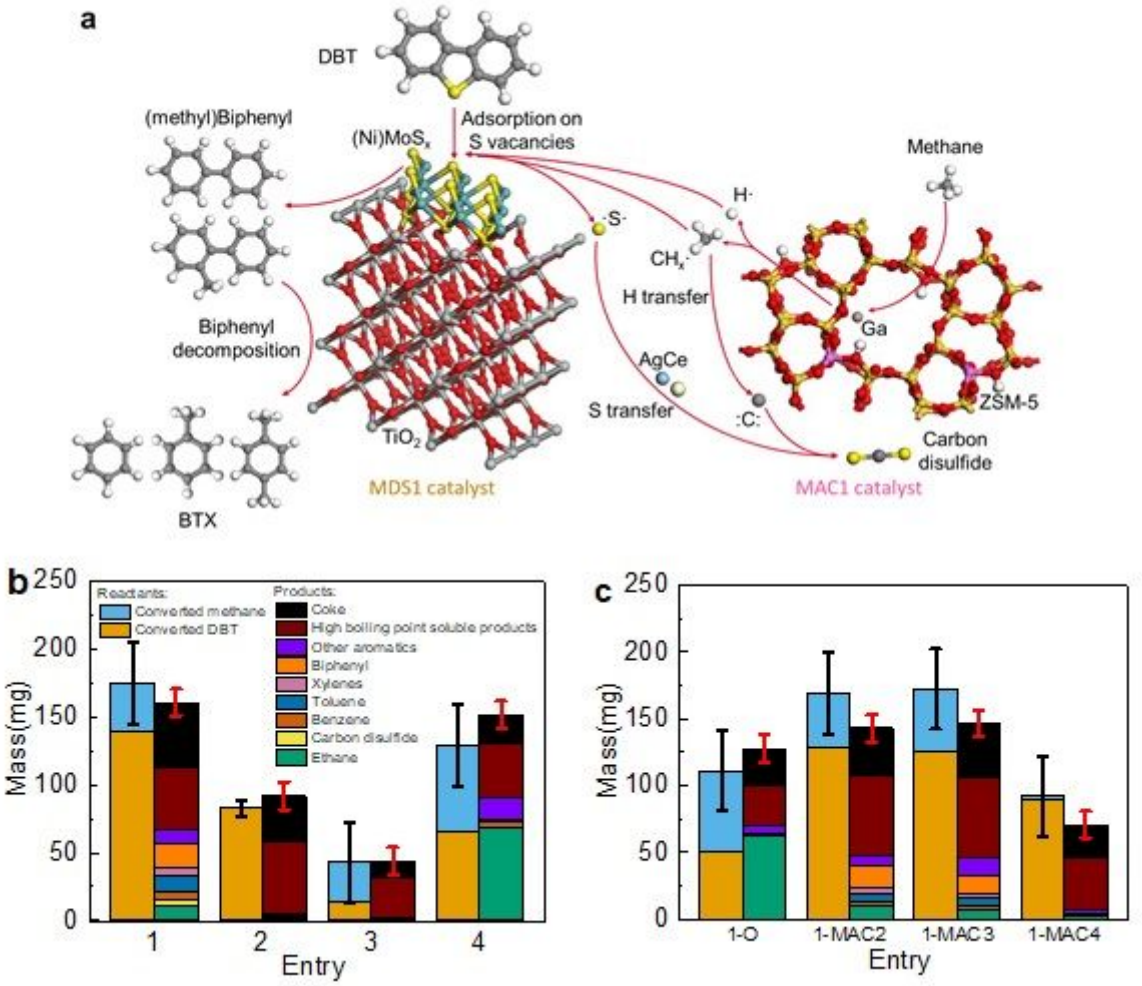

Figure 1

Mechanism illustration and reaction performances. (a) Proposed mechanism of DBT desulfurization under methane environment. Colors of atoms: yellow for S, teal for Mo, gray for C, white for H, amber for Si, magenta for Al, red for O, coral for Ga and light gray for Ti. (b, c) Quantification of converted reactants and products in entry 1 (main reaction), entry 2 (no CH4), entry 3 (no MAC1), entry 4 (no MDS1), entry 1-O (MDS1→MDS1-O), entry 1-MAC2 (MAC1→MAC2 (no Ag)), entry 1-MAC3 (MAC1→MAC3 (no Ce)) and entry 1-MAC4 (MAC1→MAC4 (no Ga)). Hydrogen is not illustrated in the columns for products because the mass contribution is negligible. The error bars represent the standard deviation for measurements.

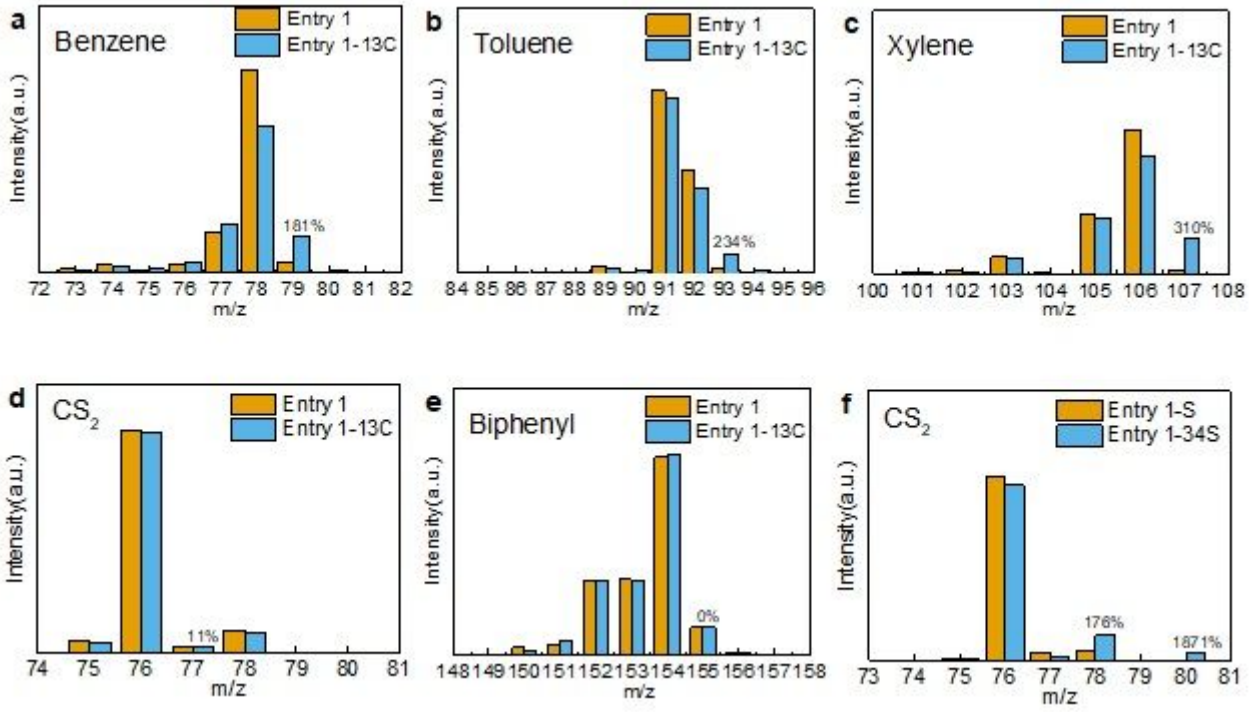

Figure 2

Mass spectra of main soluble products. (a~e) benzene, toluene, xylene, carbon disulfide and biphenyl in 13C isotope labeling experiment. (f) carbon disulfide in 34S isotope labeling experiment. The numbers above the column indicate the increase rate of signal intensities in isotope labeled entry compared to those in entry with natural isotope abundance.

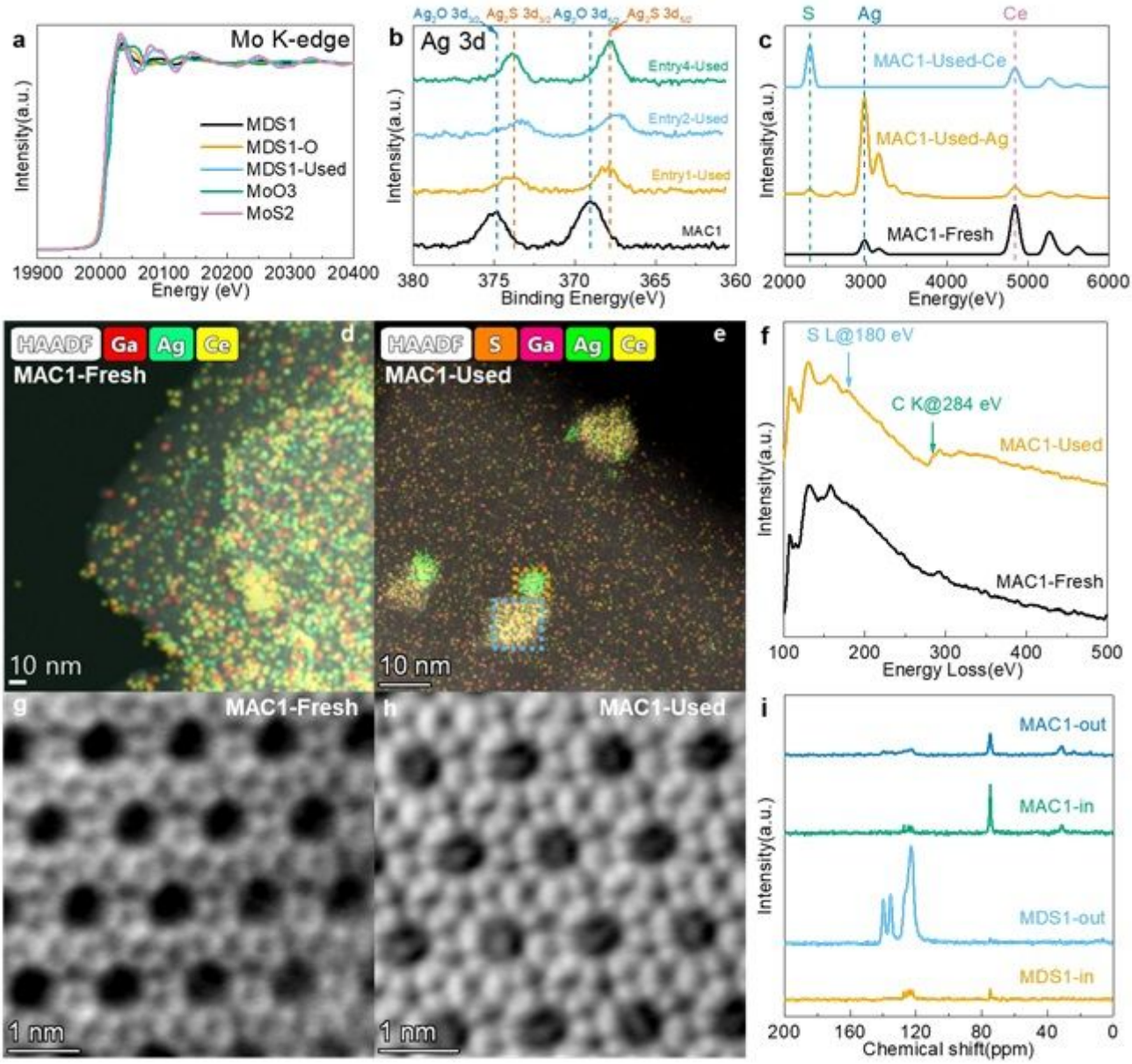

Figure 3

Catalyst characterizations. (a) Mo K-edge XAFS spectra of fresh and used MDS1 catalysts, MDS1-O catalyst and standard samples. (b) XPS spectra of fresh and used MAC1 catalysts. (c) EDX spectra of fresh and used MAC1 catalysts. The appearance of S peak can be observed in both Ag rich area (orange frame in Fig. 3(e)) and Ce rich area (blue frame in Fig. 3(e)) of the used catalysts. (d, e) EDX mapping of fresh and used MAC1 catalysts. (f) EELS of fresh and used MAC1 catalysts. (g, h) High resolution STEM-iDPC images of fresh and used MAC1 catalysts. (i) 13C{1H} SS CP/MAS NMR of vial-separated MDS1 and MAC1 catalysts after reaction. It is observed that aromatic species (120-140 ppm) are preferably adsorbed over MDS1 and aliphatic groups (25-35 ppm) are present over MAC1. More detailed explanations are given in Section 5.1, 5.3, 5.4 and 6.1 of the Supplementary Information.

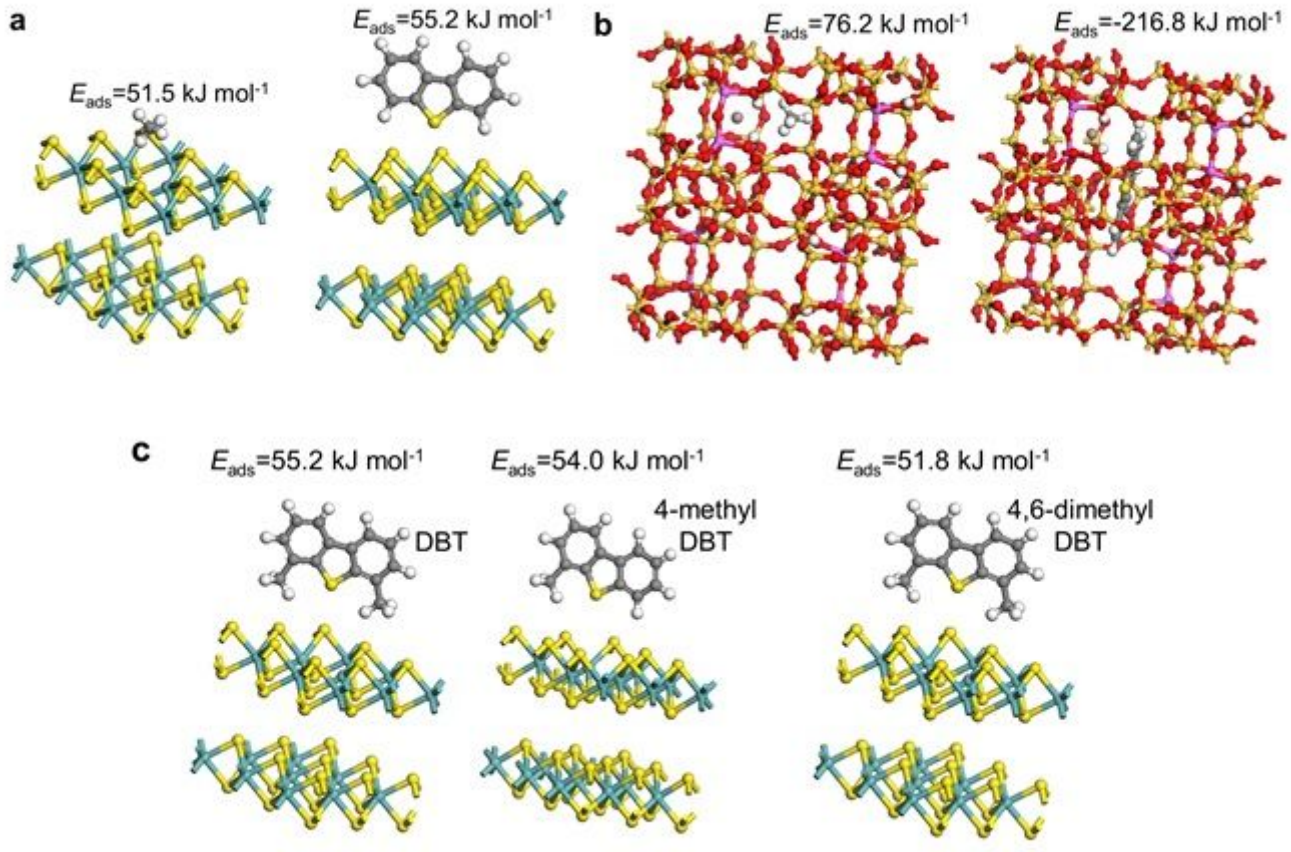

Figure 4

DFT calculations. (a) Optimized structures and adsorption energies of adsorbed methane and DBT on the sulfur vacancy of MoS2. (b) Optimized structures and adsorption energies of adsorbed methane and DBT in the inner pore of Ga/ZSM-5. (c) Optimized structures of adsorbed DBT, 4-methylDBT and 4,6-dimethylDBT on the sulfur vacancy of MoS2. The adsorption energies decrease in the order DBT > 4-methylDBT > 4,6-dimethylDBT, which is consistent with experimental results (Table S15), supporting the DDS pathway. More detailed explanations are given in Section 6 and 7 of the Supplementary Information.

Supplementary Files

This is a list of supplementary files associated with this preprint. Click to download.

- SupplementaryInformationNatureFinal.doc